Prolonged anesthesia alters brain synaptic architecture

Michael Wenzel[a,1,2], Alexander Leunig[a], Shuting Han[a], Darcy S. Peterka[a], and Rafael Yuste[a]

[a]Neurotechnology Center, Department of Biological Sciences, Columbia University, New York, NY 10027

Edited by Emery N. Brown, Massachusetts General Hospital, Boston, MA, and approved December 19, 2020 (received for review November 20, 2020)

Prolonged medically induced coma (pMIC) is carried out routinely in intensive care medicine. pMIC leads to cognitive impairment, yet the underlying neuromorphological correlates are still unknown, as no direct studies of MIC exceeding ~6 h on neural circuits exist. Here, we establish pMIC (up to 24 h) in adolescent and mature mice, and combine longitudinal two-photon imaging of cortical synapses with repeated behavioral object recognition assessments. We find that pMIC affects object recognition, and that it is associated with enhanced synaptic turnover, generated by enhanced synapse formation during pMIC, while the postanesthetic period is dominated by synaptic loss. Our results demonstrate major side effects of prolonged anesthesia on neural circuit structure.

anesthesia | dendritic spines | synaptic plasticity | memory deficit | two-photon imaging

Cognitive impairment due to prolonged medically induced coma (pMIC) represents an enormous clinical and socioeconomic burden affecting millions of patients worldwide (1–3). In adulthood, clinical trials have proven that intensive care unit (ICU) survivors frequently suffer from lasting cognitive impairment (2, 4), yet the neuromorphopathological underpinnings of this impairment have remained elusive. In early life, when the brain is highly plastic, MIC (maximum of 6 h tested in rodents to date) has been shown to result in synaptic changes and long-term cognitive impairment (5–7). However, basic animal research suggests that, during later adolescence and adulthood, dendrites and dendritic spines are stable under physiological conditions (8–10) and short-term MIC (11). Whether this notion holds true for pMIC is unknown.

Results

There has been a paucity of experimental studies of structural and functional consequences of pMIC, so we first created a robust pMIC experimental protocol for mice. We combined an anesthesia setup (Fig. 1*A*), chronic two-photon imaging of cortical synapses (Fig. 1*B*), and repeated behavioral assessment (Fig. 1*C*) into an integrated experimental framework (Fig. 1*D* and *Materials and Methods*). Two imaging sessions were carried out to determine baseline 3-d synaptic turnover (day 1, day 4). Immediately after day 4 imaging, pMIC was initiated. To document synaptic changes across pMIC, a third imaging session was performed immediately upon pMIC discontinuation (day 5). Three days post pMIC, mice were imaged once again to determine postanesthetic 3-d synaptic turnover (day 8). Additionally, a novel object recognition test was performed during baseline conditions (day 4), and repeated after recovery from pMIC (day 7) (Fig. 1*C*).

We used the inhalatory anesthetic isoflurane due to its fast kinetics and thus maximal adjustability of anesthetic depth (12). We tried to avoid an FiO_2 (fraction of inspired oxygen) >50%, as this has been associated with increased mortality in human intensive care (13). Vital parameters (peripheral O_2 saturation, heart rate, breath rate, pulse/breath distention) were continually monitored using an infrared thigh sensor (Fig. 1*E*). When developing the protocol, we successfully performed pMIC in mice for up to 40 h, yet for reasons of feasibility (continuous presence of an experimenter required), we performed pMIC on 12 adult mice (age: 7.7 ± 1.5 mo SEM) with a mean duration of 18 h (17.96 ± 0.74 SEM). Cardiorespiratory instability (after exclusion of possible sensor or detection errors: sustained non-hypovolemic hypotonic bradyarrhythmia [pulse curve, pulse/breath distension], repeated hypotonic tachycardia [self-limited], unexplained drop in O_2 saturation <90% for >30 s, sustained breath rate <30/min, repeated unexplained gasping [self-limited]) or maximum pMIC duration of 24 h were chosen as primary pMIC discontinuation criteria. Fluid and nutritional supply were ensured by administration of glucose solution (1% in phosphate-buffered saline [PBS]) via a subcutaneous line at 0.1 to 0.2 mL/hr (total volume 3.46 ± 0.35 mL SEM). Under steady-state isoflurane concentrations of 0.5 to 1.5% partial pressure in air (ppa), mice displayed continuously high peripheral oxygen saturation (96.96 ± 0.32% SEM), heart rates between 350 and 500 beats per minute (435 ± 14 SEM), breath rates of 50 to 80 excursions per minute (65 ± 3 SEM), and a pulse/breath distension ratio above 1 (1.75 ± 0.16 SEM) (Fig. 1 *E* and *F*). Oxygenation >90% was maintained with little variance across a wide range of covarying heart and breath rates (Fig. 1*E*–*G*). Breath rate showed the largest variance among monitored vital parameters (Fig. 1*G*), and most accurately clinically reflected anesthetic depth. Upon pMIC discontinuation, mice rapidly displayed accelerated heart and breath rates, and soon reacted to tactile stimulation. We defined the period between isoflurane discontinuation and first appearance of the righting reflex as wake-up time (9.65 ± 1.41 min SEM). After waking up, all mice soon showed apparently normal movement and body coordination, typical grooming, and feeding behavior. To evaluate pMIC-associated behavioral changes, mice were subjected to a novel object recognition test (14) (NOR) prior to and post pMIC (Fig. 1*C*). Expectedly, mice spent significantly

Significance

In human patients, prolonged medically induced coma (pMIC) is associated with significant cognitive deficits. Yet, a synapse-level neuromorphological correlate has been demonstrated experimentally only in early life, when the brain is highly plastic. The current notion is that synapses become increasingly stabilized and that MIC has no effect on synaptic dynamics in adulthood. Yet, the longest experimental study of MIC-associated synaptic changes has been only ~6 h. We established a pMIC experimental protocol in mice and found that pMIC alters synaptic brain architecture and object recognition at all ages. Our results ring an alarm bell to the medical community and call for the development of individually tailored anesthetic regimens and intensified research on adjuvant therapeutic strategies to maintain brain structure and function during pMIC.

Author contributions: M.W. conceived the project and designed experiments; M.W. and A.L. performed experiments; M.W., A.L., D.S.P., and S.H. analyzed data; M.W. wrote the paper; M.W., A.L., S.H., D.S.P., and R.Y. discussed results; and R.Y. assembled and directed the team.

The authors declare no competing interest.

This article is a PNAS Direct Submission.

[1]Present address: Department of Epileptology, University of Bonn, 53127 Bonn, Germany.

[2]To whom correspondence may be addressed. Email: michaelwenzel2946@gmail.com.

Published February 10, 2021.

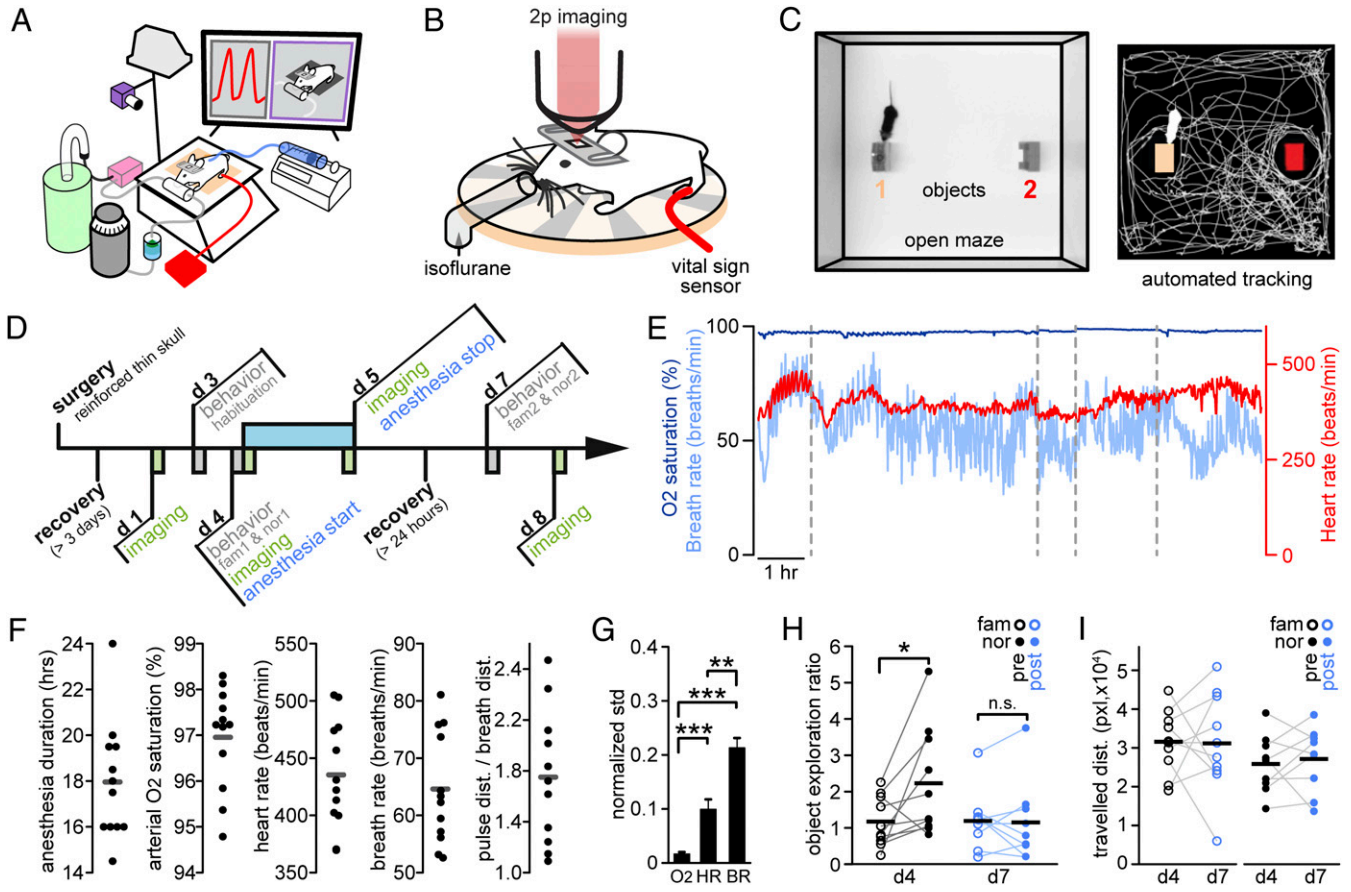

Fig. 1. Experimental design and pMIC-induced behavioral deficits. (*A*) Anesthesia setup. Mice are placed on a warming pad on a tiltable platform. Isoflurane is evaporated (dark gray) and delivered in humidified air/oxygen via a custom nose piece. Waste gas is removed by a suction pump (magenta) and trapped in a charcoal filter (green). Nutritional supply is delivered via a programmable perfusion system (blue, *Right*). An infrared lamp is placed above the setup. A thigh sensor is used for vital-sign monitoring (red). Vital signs and clinical status are live-streamed in a local network (camera, computer display). (*B*) For each imaging session, anesthetized mice are placed under the microscope, on a warming pad, under vital-sign monitoring. (*C*) Open maze for behavioral testing. Videos are recorded during FAM and NOR from above; mouse behavior is automatically tracked. (*D*) Experimental workflow. (*E*) Long-term vital-sign monitoring of an anesthetized mouse with intermittent breaks (dashed lines, e.g., for changing sensor between limbs). (*F*) Vital parameters, mean values ($n = 12$ mice), and overall mean value displayed as gray line. dist., distension. (*G*) Comparison of vital-sign normalized mean SDs ($n = 12$ mice). Unpaired *t* test with Welsh's correction: O2 saturation vs. heart rate, $P = 0.001$; O2 saturation vs. breath rate, $P < 0.0001$; heart rate vs. breath rate, $P = 0.0002$. (*H*) Relative object exploration time ratio (two objects, 50% vs. 50% = 1) during FAM (circles) and NOR (filled circles) measured during baseline (day 4), and post pMIC (day 7). Paired *t* test: FAM (day 4) vs. NOR (day 4) $P = 0.0451$ ($n = 10$ mice), FAM (day 7) vs. NOR (day 7) $P = 0.823$ ($n = 9$ mice). (*I*) Traveled distances (in pixels) prior and post pMIC during FAM (circles) and NOR (filled circles). $^*P < 0.05$, $^{**}P < 0.01$, $^{***}P < 0.001$. All bar plots show mean ± SEM.

more time exploring novel objects post familiarization (FAM) during baseline conditions (Fig. 1 *H*, *Left*). However, this effect was abolished post recovery (>24 h) from pMIC (Fig. 1 *H*, *Right*). Importantly, this could not be explained by postanesthetic reduction of locomotion, as pre- and postanesthetic total distances traveled during FAM and NOR were similar (Fig. 1*I*).

Next, we set out to study whether pMIC affects synaptic architecture. We performed repeated two-photon imaging of yellow fluorescent protein (YFP-labeled dendrites and synapses (up to ~150 µm beneath the pial surface) of layer 5 pyramidal neurons (15) in 6 of 12 adult mice undergoing pMIC (Fig. 2*A*). We used a reinforced chronic cranial window above thinned skull to minimize possible effects from invasive surgery (16). However, this reduces overall imaging fidelity, and we were unable to consistently distinguish between filopodia and dendritic spines across all imaging sessions in all mice. Therefore, we chose to focus on clearly visible synaptic protrusions, regardless of morphological classification. In six mice, we assessed a total of 1,254 synaptic protrusions (209 ± 40 SEM) on 238 dendritic compartments (40 ± 9 SEM). We noticed that, across all anesthetized mice and imaging sessions, dendrites remained stable (Fig. 2 *B* and *C*). However, pMIC-associated synapse dynamics showed considerable alterations (Fig. 2*D*). In comparison to the 1-d total synapse turnover in adult controls ($n = 6$; total synapse count: 1,113 [185.5 ± 50 SEM]), pMIC-associated synapse turnover was more than doubled ($n = 6$, total synapse count: 1,254 [209 ± 40 SEM]) (Fig. 2*E*). Both synaptic gain and loss were significantly enhanced during pMIC, with the gain of synapses outperforming their loss (Fig. 2*F*). When comparing pre- and postanesthetic 3-d synaptic turnover, turnover remained significantly enhanced after pMIC (Fig. 2*G*). In contrast to pMIC itself, the postanesthetic period was dominated by synaptic loss (Fig. 2*H*), while both postanesthetic synaptic gain and loss remained nonsignificantly increased. Intriguingly, a substantial fraction of synapses gained during pMIC remained stable across the 3-d postanesthetic period (42.69 ± 10.87% SEM [total gain: 59 synapses in $n = 6$ mice]). Relating pre- and postanesthetic synaptic turnover with change in NOR performance, we found a significant inverse relationship between increased turnover and decreased test performance (Fig. 2*I*).

Next, we put our findings in adult mice in a developmental context by examining young animals (approximately postnatal day 30). Previous research suggests that short-term MIC (maximum of

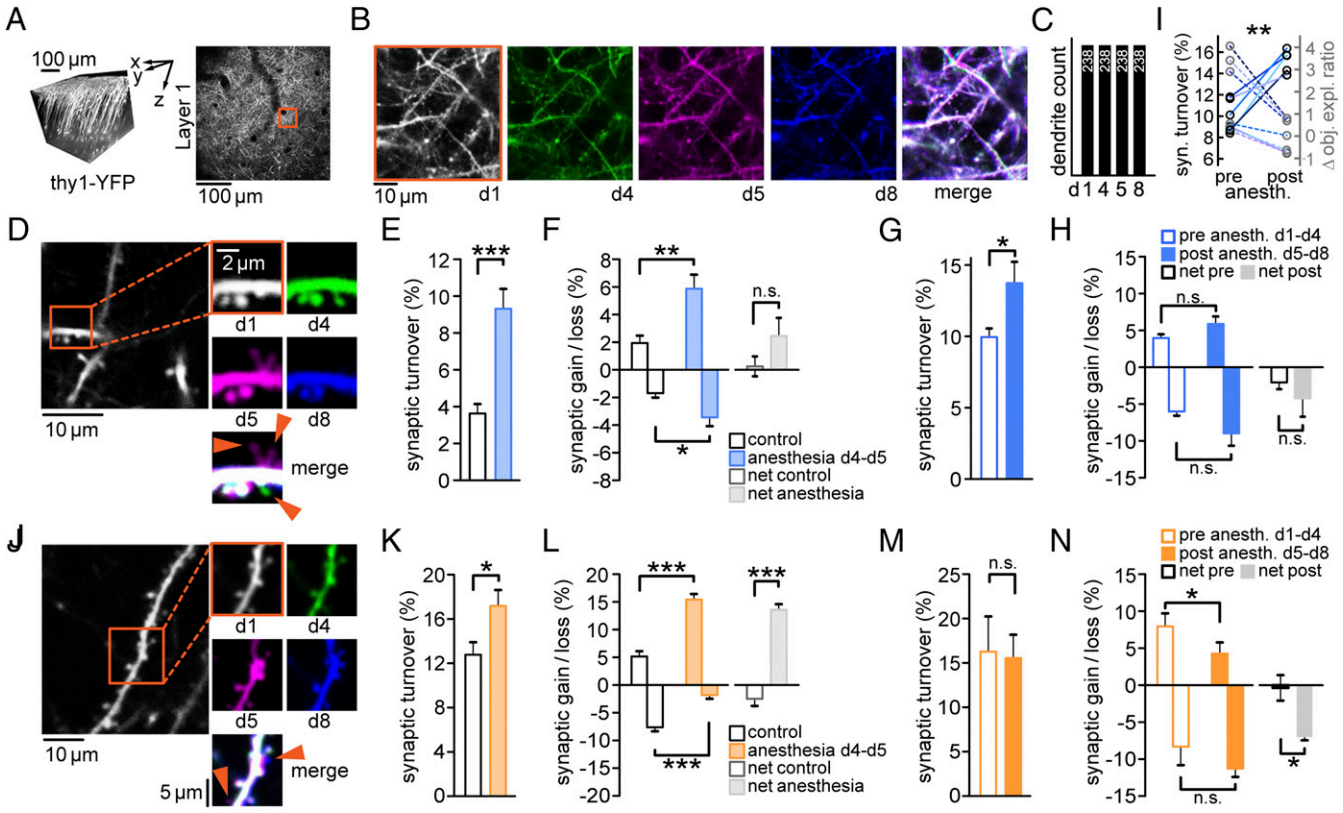

Fig. 2. pMIC leads to synaptic alterations in adolescent and adult mice. (*A*, *Left*) Three-dimensional reconstruction of imaged L5 pyramidal cells. (*A*, *Right*) Axial imaging field of view (FOV) at low magnification to re-identify zoomed-in L1 FOVs across imaging sessions by vascular landmarks. (*B*) Red *Inset* shown in *A*; identical dendritic segments were imaged four times, before pMIC (day 1, day 4), and following pMIC (day 5, day 8) in an adult mouse. (*C*) Quantification of dendritic changes across pMIC in adult mice ($n = 6$); dendritic segments remained stable. (*D*) Exemplary dendritic segment and synaptic changes across pMIC (baseline: day 1 to day 4; pMIC: day 4 to day 5; post pMIC: day 5 to day 8). Two synapses are transiently gained during pMIC (magenta), and one synapse is permanently lost (green). (*E*) Total synaptic turnover during pMIC in adult mice ($n = 6$) vs. 1-d turnover in healthy controls ($n = 6$); unpaired *t* test: $P = 0.043$. (*F*) Synaptic gain, loss, and net effect (gain – loss) during pMIC in adult mice ($n = 6$) vs. healthy controls ($n = 6$); unpaired *t* test: $P = 0.0064$ (gain), $P = 0.1728$ (net effect); Mann–Whitney *U* test: $P = 0.026$ (loss). (*G*) Total 3-d synaptic turnover ($n = 6$ adult mice) during baseline (day 1 to day 4) vs. post pMIC (day 5 to day 8); paired *t* test: $P = 0.0484$. (*H*) Synaptic gain, loss, and net effect ($n = 6$ adult mice) during baseline (day 1 to day 4) vs. post pMIC (day 5 to day 8); paired *t* test: $P = 0.4913$ (gain), $P = 0.16$ (loss), $P = 0.4441$ (net effect). (*I*) Within-mouse ($n = 6$ adult mice, one blue shade per mouse) comparison of change of synaptic turnover (black *y* axis on the *Left*; black circles and solid lines; preanesthetic vs. postanesthetic 3-d turnover) and change of NOR performance (gray *y* axis on the *Right*; gray circles and dashed lines; preanesthetic vs. postanesthetic delta object exploration ratio [FAM vs. NOR]). All mice showed a postanesthetic decrease in NOR performance, while five out of six mice showed a postanesthetic increase in synaptic turnover (Fisher's exact test: $P = 0.0076$). (*J*) Exemplary dendritic segment and synaptic changes across pMIC (baseline: day 1 to day 4; pMIC: day 4 to day 5; post pMIC: day 5 to day 8). Two synapses are gained during pMIC (magenta) and persist post pMIC (blue). (*K*) Total synaptic turnover during pMIC in young mice ($n = 4$) vs. 1-d turnover in healthy controls ($n = 5$); unpaired *t* test: $P = 0.0433$. (*L*) Synaptic gain, loss, and net effect during pMIC in young mice ($n = 4$) vs. healthy controls ($n = 5$); unpaired *t* test: $P = 0.0002$ (gain), $P = 0.0007$ (loss), $P < 0.0001$ (net effect). (*M*) Total 3-d synaptic turnover ($n = 4$ young mice) during baseline (day 1 to day 4) vs. post pMIC (day 5 to day 8); paired *t* test: $P = 0.7099$. (*N*) Synaptic gain, loss, and net effect ($n = 4$ young mice) during baseline (day 1 to day 4) vs. post pMIC (day 5 to day 8); paired *t* test: $P = 0.043$ (gain), $P = 0.1671$ (loss), $P = 0.0386$ (net effect). $^*P < 0.05$, $^{**}P < 0.01$, $^{***}P < 0.001$. All bar plots show mean ± SEM.

6 h tested) at a young age (≤ 1 mo in rodents) is associated with long-term cognitive impairment (7), and increased synapse formation is associated with an age-dependent decreasing effect size (no effect on dendritic spines at age >1 mo) (5, 6, 11).

Similarly to adult mice, pMIC in young mice ($n = 4$, pMIC duration = 18.5 ± 1.26 h SEM) was associated with enhanced 1-d synapse turnover (Fig. 2 *J* and *K*; $n = 4$ mice; total synapse count: 284 [71 ± 12 SEM]). In line with previous results on immature synapses in 1-mo-old mice (isoflurane for 4 h) (11), synaptic loss was significantly reduced during pMIC compared to controls (Fig. 2*L*; $n = 5$ mice; total synapse count: 587 [117.4 ± 15 SEM]). At the same time, consistent with our results for pMIC in adult mice, pMIC-associated synapse formation was strongly increased, resulting in a pronounced net-positive synaptic turnover (Fig. 2*L*). When comparing pre- and postanesthetic 3-d synaptic turnover, total turnover remained unchanged (Fig. 2*M*). Yet, in contrast to adult mice, synaptic formation post pMIC in younger mice was significantly reduced and synapse elimination increased, resulting in a net-negative synaptic turnover (Fig. 2*N*). Again, a substantial fraction of synapses gained during pMIC remained stable during the postanesthetic period (50.57 ± 9.09% SEM [total gain: 36 synapses in $n = 4$ mice]).

Discussion

Our data demonstrate that prolonged general anesthesia in mice alters object recognition and cortical synaptic architecture at all ages. With isoflurane, we find net-positive synapse turnover during pMIC, followed by a net-negative synapse turnover during the postanesthetic period. Across all examined ages, a substantial fraction of newly formed spines during pMIC displayed post-anesthetic stability, suggesting that they may form persistent synaptic connections. Given the relevance of synapses and experience-driven synaptic plasticity for cognitive function and memory (17, 18), our observation of pMIC-associated synaptic dynamics represents

a possible factor contributing to memory impairment following pMIC. The mechanisms underlying these alterations likely play out across multiple anatomical scales (19). On the molecular level, anesthetics target ion channels (20). On the organelle level, anesthetics exert effects, e.g., on a cell's cytoskeleton (21). Ultimately, circuit-level alterations may play a main role in pMIC-associated synaptic dynamics, since prolonged pharmacological circuit inactivation may interfere with physiological synaptic changes associated with intrinsic (e.g., circadian protein expression) (22) and extrinsic environmental parameters (e.g., novel sensory experience) across age (23).

A limitation of this study is whether our synaptic-level findings translate to human pMIC, as such studies do not yet exist. However, recent progress in positron emission tomography imaging of synaptic density in humans using synapse-specific radioligands (24–26) could enable future studies on pMIC-associated synaptic changes even in humans, all other logistical complications of such an enterprise aside. Another possible limitation of the present study is that we examined synaptic plasticity in sensory cortex, but not in higher order cortices. We chose somatosensory cortex for several reasons. In addition to its accessibility for high-resolution imaging, it represents the most extensively studied murine brain area in the field of synaptic plasticity, and thus enables contextualization of our results in light of a prominent body of literature on synaptic stability in adulthood (8–11, 27–30). Furthermore, particularly in mice, somatosensory cortex is important for exploration and tactile learning (31–33), object discrimination, and recognition (34, 35), and thus represents a logical imaging target for pMIC-associated behavioral changes. In addition, sensory cortices contribute to cognitive function (36). Primary sensory and higher-order cortices share reciprocal connections (37–39), and recent work suggests that sensory cortices also implement internal representations of the external environment, even in the absence of specific stimuli (40, 41). Further evidence of the sensory cortex playing a role in working memory (42), social contextualization of conspecifics (43), and reward-related task-relevant anticipation (44) points toward an associative capacity of sensory cortices beyond their immediate sensory function. However, as in addition to basic cognitive impairment (measured e.g. by RBANS assessment) (45), intensive care unit survivors often suffer from impaired executive function (2), the study of higher-level cognitive abilities is of significant interest for further synapse-level research on pMIC. Future steps in this direction will require more specific behavioral testing, and more invasive imaging strategies, e.g. in hippocampus (46, 47) or medial prefrontal cortex (mPFC) (48, 49). In this context, it is important to keep in mind that the longitudinal in vivo synapse dynamics of the hippocampus and mPFC (49–51) are far less well understood than those in sensory cortex. As we imaged somatosensory cortex for the above-mentioned reasons, there is no definitive proof yet that the results reported here extend to other brain areas, too. However, given that anesthetics are administered systemically, and thus distribute throughout the entire brain, it is much rather likely than not that other brain areas will show similar, even if to a different degree, pMIC-associated synaptic changes.

Together, the findings of this pilot study carry important implications for medical care, as they point out significant structural and functional side effects of pMIC. They further indicate that, with regards to pMIC, the synaptic architecture of the adult brain is less stable than previously thought, which has major implications for general anesthesia in intensive care medicine. To date, no standard approach exists to prevent cognitive side effects or alterations of brain architecture during pMIC. For this study, we chose the inhalatory anesthetic isoflurane, which is part of a common class of anesthetics in anesthesiology (52), is widely established in animal research, can be administered non-invasively, does not accumulate in the body, and has a short elimination half-life enabling high controllability of anesthetic depth (53). Partly due to this, inhalatory anesthetics have experienced a renaissance in intensive care medicine using AnaConDa or Mirus systems (53–55). The results of this study make the case for a systematic investigation of synapse-level effects and related cognitive impairment triggered by commonly used anesthetics in intensive care, including propofol and benzodiazepines, and particularly combinations of anesthetics. A better understanding of pMIC-related effects on cortical synapses could allow for more individually tailored anesthetic regimens (52) and could foster research on adjuvant therapeutic strategies to improve cognitive outcomes of ICU survivors.

Materials and Methods

General Information. All experiments were carried out in compliance with the Columbia University institutional animal care guidelines. We used B6.Cg-Tg(Thy1-YFP)HJrs/J mice (15) (Jackson Laboratories; Research Resource Identifier IMSR_JAX:003782), where cortical layer 5 pyramidal neurons are preferentially labeled. For experiments, the postnatal age of mice ranged from 1 to 12 mo (two age groups: postnatal days 30 to 35 [pMIC/imaging: two females, two males; control/imaging: two females, three males], or postnatal days 120 to 360 [pMIC: four females, eight males; pMIC/behavior: three females, seven males; pMIC/behavior/imaging: one female, five males; control/imaging: two females, four males]). Mice were housed at a 12-h light/dark cycle, and food and water were provided ad libitum.

Surgical Procedures. For repeated two-photon imaging of cortical synapses, a reinforced thin skull chronic cranial window was established as described (56). We chose a "thin skull" approach to minimize potential craniotomy-related changes of synaptic plasticity that have been reported previously (16). In brief, mice were anesthetized with isoflurane (initial dose 2 to 3% partial pressure in air followed by reduction to 1 to 1.5%). Prior to surgery, all mice received carprofen subcutaneously (s.c.), enrofloxacin (s.c.), and dexamethasone (intramuscularly). Throughout surgical procedures, proper anesthetic depth was checked intermittently by toe and tail pinching. Under sterile conditions, a small flap of skin above the skull was removed, and a titanium head plate with a central foramen (7 × 7 mm) was fixed on the skull using dental cement. Then, a dental microdrill was used at low rotation speed to carefully thin a small region (usually <1 mm in diameter) over the left somatosensory cortex. To prevent the skull and brain tissue from heating up by the drilling process, drilling and wetting with sterile artificial cerebrospinal fluid (ACSF) were alternated frequently. At a thickness of around 50 μm, the skull typically began to bend upon gentle pressure and the intracranial vasculature became clearly visible under the moistened skull. In addition, small air bubbles within the thin spongioform part of the thinned skull appeared when ACSF was applied. From here on, the skull was further thinned at an even lower drilling rotation speed and with minimal vertical pressure, down to a thickness of 10 to 20 μm. When thin enough, the small air enclosures in the skull no longer appeared upon ACSF application.

At this point, the skull was allowed to dry completely. Once dry, a small drop of cyanoacrylate glue was applied onto the thinned skull. Immediately following the application of the glue, a thin glass coverslip (3 mm in diameter, no. 0, Warner Instruments) was lowered and gently pressed onto the thinned area, held in place by a stereotactic arm. After glue solidification (several minutes), the edges of the glass coverslip were sealed off by dental cement. Following the surgical procedure, mice received pain medication and were allowed to recover for at least 3 d. The "reinforcement" of the cranial window prevented the skull from growing back, making it possible to image the same cortical structures repeatedly without the need of re-thinning the skull.

Experimental Time Line. The experimental time line is displayed in Fig. 1*D*. Following recovery from surgical establishment of a chronic cranial window, mice were acclimatized to the experimenter until no signs of distress were present (usually approximately three sessions of 30 min each). Then, two imaging sessions were carried out to determine the baseline 3-d synaptic turnover (day 1, day 4). In between baseline imaging sessions, mice were habituated to the open field maze (day 3) and subjected to a first novel object recognition test (14) (NOR1, day 4). Immediately post imaging on day 4, pMIC was initiated. To document synaptic changes occurring during pMIC, a third imaging session was carried out right at the end of pMIC (day 5). After at least 24 h of recovery from pMIC, mice were subjected to a second

NOR (NOR2, day 7). Three days after pMIC termination, mice were imaged once again to determine their postanesthetic 3-d synaptic turnover (day 8).

Prolonged Medically Induced Coma. The tightly controlled and safe pMIC procedure (−24 h) required the continuous presence of an experimenter. Mimicking hospital conditions, remote video and vital parameter monitoring allowed the experimenter to leave the pMIC setup while maintaining the ability to rapidly carry out setup adjustments. Based on a protocol of long-term anesthesia in mice (57), we established a setup that permits continuous general anesthesia of mice for up to several days (Fig. 1*A*). While anesthetized, mice were kept on a warming pad maintaining a body core temperature of 37.5 °C through a rectal probe and closed-loop temperature control system (ATC2000, World Precision Instruments). The warming pad was placed on a tiltable platform whose angle was slightly changed intermittently (maximum 4°) in order to shift the animals' center of mass to reduce pressure pain and bruising. As mice lose body temperature easily due to their anatomy, an infrared lamp was additionally put in place and optionally switched on, if needed. Isoflurane was delivered in humidified air through a custom nose piece (initial dose: 1.5 to 2.5% ppa; steady-state dose: 0.5 to 1.5% ppa). Ventilation air was humidified between the isoflurane vaporizer and the nose piece, and all waste gas was actively removed via a suction pump. With the help of a dual gas flowmeter system (100% O_2 and room air) set up before the isoflurane vaporizer system, the oxygen fraction (FiO_2) in air could be modified seamlessly between 21 and 100%. FiO_2 adjustment depended on the measured peripheral arterial O_2 saturation. During the early period of pMIC, a fraction of inspired oxygenation (FiO_2) of 21% was completely sufficient to maintain high peripheral O_2 saturation in all anesthetized mice, while subsequently (>8 h), FiO_2 was usually slowly increased toward pMIC termination without exceeding 50%. Similarly to human intensive care, we tried to avoid an FiO_2 >50% (13). To provide the animal with sufficient fluid and nutrition during anesthesia, continuous fluid (saline) and nutritional supply (1% glucose solution in PBS) were administered via a programmable perfusion system through a subcutaneous line at a rate of 0.1 to 0.2 mL/h. All throughout anesthesia, basic vital parameters (blood oxygenation, heart rate, breath rate, pulse distension, breath distension) were continuously monitored and recorded by a thigh or paw sensor (mouse ox plus system, Starr Life Sciences). The sensor was periodically moved from one extremity to another to reduce pressure-induced tissue damage. Technically erroneous vital sign data points (e.g. due to visible thigh compression by the sensor clip, confirmed by immediate normalization of vital signs upon moving the clip to another limb) were excluded from analysis. A sustained pulse/breath distension ratio below 1 was sought to be avoided (57), as it indicates that anesthesia is too deep (large inhalatory excursions and gasping in combination with brady- or normocardia) or a lack of intravascular fluid (hypovolemia in combination with tachycardia). The experimenter was continually present in the laboratory to perform imaging immediately prior and post pMIC, and to adjust, for example, anesthetic depth or fluid supply with minimal delay all throughout anesthesia. Real-time streaming of video monitoring (Thorlabs, DCC1645C) and vital parameters through a local network allowed for remote monitoring of anesthetized animals.

Two-Photon Imaging. For chronic surveillance of structural synaptic changes in vivo, dendritic arborization, and dendritic spines of layer 5 cortical neurons expressing YFP (15) were imaged four times (day 1, day 4 [start of anesthesia], day 5 [end of anesthesia], day 8) using a two-photon microscope (Bruker Ultima) and a Ti:Sapphire laser (Chameleon Ultra II; Coherent) at 940 nm through a 25x objective (water immersion, numerical aperture: 1.05; Olympus). Galvanometer scanning and image acquisition was controlled by Prairie View Imaging software. Each imaging session (~15 to 30 min) included one to four high-resolution z-stacks in different locations (field of view typically ~50 × 50 μm, 512 × 512 pixels, step size 1.5 μm, stack depth up to 150 μm beneath the pial surface). Imaged z-stacks were precisely coregistered across each imaging session by vascular landmarks and several different optical zoom average images of the cortex. For each imaging session, head-restrained animals were kept under light isoflurane anesthesia (0.5 to 1% partial pressure in air) via a nose piece while body temperature was maintained with a warming pad (37.5 °C).

Novel Object Recognition Test. Before and after anesthesia, mice were subjected to basic cognitive testing by use of a NOR test, a widely used basic measure of cognitive function and recognition memory in mice (14). Following habituation (experimental day 3, Fig. 1*D*) to an open field maze (50 × 50 cm), mice underwent a first NOR (experimental day 4, prior to start of pMIC). Initially, mice were exposed to two identical objects (e.g., cell culture flasks filled with sand or LEGO towers) that were placed in the open field for 10 min ("familiarization", FAM). After FAM, mice returned to their home cage for 4 to 5 h after which they were placed in the open field maze again, yet with one of the two identical objects replaced by a novel object (differently shaped flask or LEGO tower, respectively). After pMIC, FAM and NOR were repeated for each mouse with the complementary, previously unused set of flasks or LEGO tower objects at least 24 h after pMIC termination (experimental day 7), so changes in recognition memory could be evaluated. All behavioral testing was videotaped (7.5 fr/s) from above the open field. We used custom written Matlab code for automated tracking (traveled distance, object exploration time) of mouse exploratory behavior during FAM and NOR (Fig. 1*C*).

Data Analysis. Similarly to previously described procedures for quantifying synapse dynamics (58), stacks were analyzed using the freely available software ImageJ (http://rsbweb.nih.gov/ij/). Individual 3-d stacks for each time point (day 1, day 4, day 5, day 8) and imaged areas (one to four per animal) were analyzed side-by-side by two examiners who were blinded to conditions, except for the reference imaging time point (day 1). Based on consensus between the two blinded examiners, clearly visible protrusions on dendritic segments were classified as synapses. For each dendritic segment analyzed, same synapses were defined as present (1) or absent (0) across stacks (imaging time points). Based on the examiners' consensus, synapses could be defined as stable, gained, or eliminated across (blinded) imaging time points. Once an entire experiment was analyzed, real imaging time points could be revealed and thus reassigned to individual stacks. Upon testing for normality using a Kolmogorov–Smirnov test statistic, statistical differences between synaptic turnover and synaptic gain or loss were examined using paired (pre- vs. postanesthetic) or unpaired (control group vs. anesthetized group) Student's *t* test, unless stated otherwise. The relationship (decrease or increase) between pre- vs. postanesthetic synaptic turnover and pre- vs. postanesthetic NOR performance was statistically analyzed using Fisher's exact test. All statistical analyses were carried out using MATLAB-R2017b (MathWorks) and Prism 5 (GraphPad Software).

Data Availability. All study data included in the paper are available from the corresponding author upon reasonable request. The custom MATLAB code for automated behavioral tracking is available at https://github.com/hanshuting/mnovobj.

ACKNOWLEDGMENTS. We thank R.Y. laboratory members for useful comments and Prof. H.W. Pfister (LMU, Munich) for clinical supervision. This work was supported by the National Eye Institute (R01EY011787) and National Institute of Mental Health (R01MH115900). M.W. is a Hertie Fellow in the Hertie Network of Excellence in Clinical Neuroscience. R.Y. is an Ikerbasque Research Professor at the Donostia International Physics Center.

1. C. E. Cox, S. S. Carson, Medical and economic implications of prolonged mechanical ventilation and expedited post-acute care. *Semin. Respir. Crit. Care Med.* **33**, 357–361 (2012).
2. P. P. Pandharipande *et al.*; BRAIN-ICU Study Investigators, Long-term cognitive impairment after critical illness. *N. Engl. J. Med.* **369**, 1306–1316 (2013).
3. M. Unroe *et al.*, One-year trajectories of care and resource utilization for recipients of prolonged mechanical ventilation: A cohort study. *Ann. Intern. Med.* **153**, 167–175 (2010).
4. J. Kohler *et al.*, Cognitive deficits following intensive care. *Dtsch. Arztebl. Int.* **116**, 627–634 (2019).
5. A. Briner *et al.*, Developmental stage-dependent persistent impact of propofol anesthesia on dendritic spines in the rat medial prefrontal cortex. *Anesthesiology* **115**, 282–293 (2011).
6. M. De Roo *et al.*, Anesthetics rapidly promote synaptogenesis during a critical period of brain development. *PLoS One* **4**, e7043 (2009).
7. R. D. Sanders, J. Hassell, A. J. Davidson, N. J. Robertson, D. Ma, Impact of anaesthetics and surgery on neurodevelopment: An update. *Br. J. Anaesth.* **110** (suppl. 1), i53–i72 (2013).
8. J. Grutzendler, N. Kasthuri, W. B. Gan, Long-term dendritic spine stability in the adult cortex. *Nature* **420**, 812–816 (2002).
9. Y. Zuo, A. Lin, P. Chang, W. B. Gan, Development of long-term dendritic spine stability in diverse regions of cerebral cortex. *Neuron* **46**, 181–189 (2005).
10. J. T. Trachtenberg *et al.*, Long-term in vivo imaging of experience-dependent synaptic plasticity in adult cortex. *Nature* **420**, 788–794 (2002).
11. G. Yang, P. C. Chang, A. Bekker, T. J. J. Blanck, W. B. Gan, Transient effects of anesthetics on dendritic spines and filopodia in the living mouse cortex. *Anesthesiology* **115**, 718–726 (2011).
12. N. Yasuda *et al.*, Kinetics of desflurane, isoflurane, and halothane in humans. *Anesthesiology* **74**, 489–498 (1991).

13. E. de Jonge *et al*., Association between administered oxygen, arterial partial oxygen pressure and mortality in mechanically ventilated intensive care unit patients. *Crit. Care* **12**, R156 (2008).
14. M. Leger *et al*., Object recognition test in mice. *Nat. Protoc.* **8**, 2531–2537 (2013).
15. G. Feng *et al*., Imaging neuronal subsets in transgenic mice expressing multiple spectral variants of GFP. *Neuron* **28**, 41–51 (2000).
16. H. T. Xu, F. Pan, G. Yang, W. B. Gan, Choice of cranial window type for in vivo imaging affects dendritic spine turnover in the cortex. *Nat. Neurosci.* **10**, 549–551 (2007).
17. M. Segal, Dendritic spines: Morphological building blocks of memory. *Neurobiol. Learn. Mem.* **138**, 3–9 (2017).
18. R. Yuste, Dendritic spines and distributed circuits. *Neuron* **71**, 772–781 (2011).
19. P. Århem, G. Klement, J. Nilsson, Mechanisms of anesthesia: Towards integrating network, cellular, and molecular level modeling. *Neuropsychopharmacology* **28** (suppl. 1), S40–S47 (2003).
20. M. D. Krasowski, N. L. Harrison, General anaesthetic actions on ligand-gated ion channels. *Cell. Mol. Life Sci.* **55**, 1278–1303 (1999).
21. S. Kaech, H. Brinkhaus, A. Matus, Volatile anesthetics block actin-based motility in dendritic spines. *Proc. Natl. Acad. Sci. U.S.A.* **96**, 10433–10437 (1999).
22. C. Liston *et al*., Circadian glucocorticoid oscillations promote learning-dependent synapse formation and maintenance. *Nat. Neurosci.* **16**, 698–705 (2013).
23. M. Fu, Y. Zuo, Experience-dependent structural plasticity in the cortex. *Trends Neurosci.* **34**, 177–187 (2011).
24. F. Bretin *et al*., Biodistribution and radiation dosimetry for the novel SV2A radiotracer [(18)F]UCB-H: First-in-Human study. *Mol. Imaging Biol.* **17**, 557–564 (2015).
25. J. Mercier *et al*., Discovery of heterocyclic nonacetamide synaptic vesicle protein 2A (SV2A) ligands with single-digit nanomolar potency: Opening avenues towards the first SV2A positron emission tomography (PET) ligands. *ChemMedChem* **9**, 693–698 (2014).
26. S. J. Finnema *et al*., Imaging synaptic density in the living human brain. *Sci. Transl. Med.* **8**, 348ra96 (2016).
27. A. Holtmaat, L. Wilbrecht, G. W. Knott, E. Welker, K. Svoboda, Experience-dependent and cell-type-specific spine growth in the neocortex. *Nature* **441**, 979–983 (2006).
28. S. B. Hofer, T. D. Mrsic-Flogel, T. Bonhoeffer, M. Hübener, Experience leaves a lasting structural trace in cortical circuits. *Nature* **457**, 313–317 (2009).
29. L. Ma *et al*., Experience-dependent plasticity of dendritic spines of layer 2/3 pyramidal neurons in the mouse cortex. *Dev. Neurobiol.* **76**, 277–286 (2016).
30. C. Liston, W. B. Gan, Glucocorticoids are critical regulators of dendritic spine development and plasticity in vivo. *Proc. Natl. Acad. Sci. U.S.A.* **108**, 16074–16079 (2011).
31. N. J. Sofroniew, K. Svoboda, Whisking. *Curr. Biol.* **25**, R137–R140 (2015).
32. N. Pacchiarini, K. Fox, R. C. Honey, Perceptual learning with tactile stimuli in rodents: Shaping the somatosensory system. *Learn. Behav.* **45**, 107–114 (2017).
33. N. J. Sofroniew, J. D. Cohen, A. K. Lee, K. Svoboda, Natural whisker-guided behavior by head-fixed mice in tactile virtual reality. *J. Neurosci.* **34**, 9537–9550 (2014).
34. M. Antunes, G. Biala, The novel object recognition memory: Neurobiology, test procedure, and its modifications. *Cogn. Process.* **13**, 93–110 (2012).
35. E. Guic-Robles, W. M. Jenkins, H. Bravo, Vibrissal roughness discrimination is barrelcortex-dependent. *Behav. Brain Res.* **48**, 145–152 (1992).
36. D. Mumford, On the computational architecture of the neocortex. II. The role of cortico-cortical loops. *Biol. Cybern.* **66**, 241–251 (1992).
37. D. J. Felleman, D. C. Van Essen, Distributed hierarchical processing in the primate cerebral cortex. *Cereb. Cortex* **1**, 1–47 (1991).
38. G. Minamisawa, S. E. Kwon, M. Chevée, S. P. Brown, D. H. O'Connor, A non-canonical feedback circuit for rapid interactions between somatosensory cortices. *Cell Rep.* **23**, 2718–2731.e6 (2018).
39. S. A. Bedwell, E. E. Billett, J. J. Crofts, C. J. Tinsley, The topology of connections between rat prefrontal, motor and sensory cortices. *Front. Syst. Neurosci.* **8**, 177 (2014).
40. P. Berkes, G. Orbán, M. Lengyel, J. Fiser, Spontaneous cortical activity reveals hallmarks of an optimal internal model of the environment. *Science* **331**, 83–88 (2011).
41. J. E. Miller, I. Ayzenshtat, L. Carrillo-Reid, R. Yuste, Visual stimuli recruit intrinsically generated cortical ensembles. *Proc. Natl. Acad. Sci. U.S.A.* **111**, E4053–E4061 (2014).
42. A. Fassihi, A. Akrami, V. Esmaeili, M. E. Diamond, Tactile perception and working memory in rats and humans. *Proc. Natl. Acad. Sci. U.S.A.* **111**, 2331–2336 (2014).
43. E. Bobrov, J. Wolfe, R. P. Rao, M. Brecht, The representation of social facial touch in rat barrel cortex. *Curr. Biol.* **24**, 109–115 (2014).
44. C. O. Lacefield, E. A. Pnevmatikakis, L. Paninski, R. M. Bruno, Reinforcement learning recruits somata and apical dendrites across layers of primary sensory cortex. *Cell Rep.* **26**, 2000–2008.e2 (2019).
45. C. Randolph, M. C. Tierney, E. Mohr, T. N. Chase, The repeatable battery for the assessment of neuropsychological status (RBANS): Preliminary clinical validity. *J. Clin. Exp. Neuropsychol.* **20**, 310–319 (1998).
46. D. A. Dombeck, C. D. Harvey, L. Tian, L. L. Looger, D. W. Tank, Functional imaging of hippocampal place cells at cellular resolution during virtual navigation. *Nat. Neurosci.* **13**, 1433–1440 (2010).
47. W. Yang *et al*., Anesthetics fragment hippocampal network activity, alter spine dynamics and affect memory consolidation. *bioRxiv* [Preprint] (2021). https://doi.org/10.1101/2020.06.05.135905 (accessed 8 February 2021).
48. R. J. Low, Y. Gu, D. W. Tank, Cellular resolution optical access to brain regions in fissures: Imaging medial prefrontal cortex and grid cells in entorhinal cortex. *Proc. Natl. Acad. Sci. U.S.A.* **111**, 18739–18744 (2014).
49. R. N. Moda-Sava *et al*., Sustained rescue of prefrontal circuit dysfunction by antidepressant-induced spine formation. *Science* **364**, eaat8078 (2019).
50. L. Gu *et al*., Long-term in vivo imaging of dendritic spines in the hippocampus reveals structural plasticity. *J. Neurosci.* **34**, 13948–13953 (2014).
51. T. Pfeiffer, Super-resolution STED and two-photon microscopy of dendritic spine and microglial dynamics. *University of Bordeaux*, https://tel.archives-ouvertes.fr/tel-01967610 (2017).
52. E. N. Brown, K. J. Pavone, M. Naranjo, Multimodal general anesthesia: Theory and practice. *Anesth. Analg.* **127**, 1246–1258 (2018).
53. P. V. Sackey, C. R. Martling, F. Granath, P. J. Radell, Prolonged isoflurane sedation of intensive care unit patients with the Anesthetic Conserving Device. *Crit. Care Med.* **32**, 2241–2246 (2004).
54. M. Bellgardt *et al*., Use of MIRUS™ for MAC-driven application of isoflurane, sevoflurane, and desflurane in postoperative ICU patients: A randomized controlled trial. *Ann. Intensive Care* **9**, 118 (2019).
55. A. Jerath *et al*., The use of volatile anesthetic agents for long-term critical care sedation (VALTS): Study protocol for a pilot randomized controlled trial. *Trials* **16**, 560 (2015).
56. P. J. Drew *et al*., Chronic optical access through a polished and reinforced thinned skull. *Nat. Methods* **7**, 981–984 (2010).
57. A. J. Ewald, Z. Werb, M. Egeblad, Monitoring of vital signs for long-term survival of mice under anesthesia. *Cold Spring Harb. Protoc.* **2011**, pdb.prot5563 (2011).
58. G. Yang, F. Pan, W. B. Gan, Stably maintained dendritic spines are associated with lifelong memories. *Nature* **462**, 920–924 (2009).